IFAC

Optimal Feed Forward Profiles for Dynamic Flying Height Control in Hard Disk Drives

Uwe Boettcher * **Hui Li** ** **Raymond A. de Callafon** ***
Frank E. Talke ****

* *University of California, San Diego, Center for Magnetic Recording
Research , 9500 Gilman Drive, Mail Code 0401, La Jolla , CA 92093,
U.S.A. (e-mail: uwe@ucsd.edu)*
** *Storage Mechanics Laboratory, Hitachi Asia Ltd., Singapore 049318,
Singapore (email: hli@has.hitachi.com.sg)*
*** *University of California, San Diego Dept. of Mechanical and
Aerospace Engineering, 9500 Gilman Drive, Mail Code 0411, La Jolla,
CA 92093, U.S.A. (e-mail: callafon@ucsd.edu)*
**** *University of California, San Diego, Center for Magnetic
Recording Research , 9500 Gilman Drive, Mail Code 0401, La Jolla ,
CA 92093, U.S.A. (e-mail: ftalke@ucsd.edu)*

Abstract: A dynamic model of the resistance heater in a thermal flying height control (TFC) slider of a hard disk drive is identified and used for dynamic flying height control. Experimental data obtained on a spin stand and the generalized realization algorithm are used for identification of a discrete-time dynamic model of the resistance heater (thermal actuator). The flying height change is measured using servo burst information written onto the disk surface. Based on the identified discrete-time model of the heater and convex optimization techniques, a computational scheme is proposed to obtain optimized feed forward input profiles to the heater element that minimize repeatable flying height variations and enable low flying heights.

Keywords: Reliable measurement and actuation; Modeling; Microsystems: nano- and micro-technologies

1. INTRODUCTION

Since the first hard disk drive (HDD) was introduced in 1956, the storage density has increased over eight orders of magnitudes (Hsia (2006)). One of the enabling technologies is the reduction of the clearance between the read/write element and the recording medium and the minimization of flying height variations to maintain low bit error rates (Tang et al. (2007)). The flying height has decreased from about 20 μm (Harker et al. (1981)) to a few nanometers in today's HDDs. The idea of actively controlling the flying height was introduced many years ago by Yeack-Scranton et al. (1990). Resistance heater elements for flying height control were introduced by Mächtle et al. (2001). The implementation of this feature became necessary at low flying heights for various reasons. First, the write head causes thermal deformation of the air bearing surface towards the disk during the write process. This causes a different flying height during writing and reading, respectively, which is not desired. To mitigate this effect; and achieve the same flying height during reading and writing, heads were introduced that feature a resistance heater element that is positioned in close proximity to the read/write element. Figure 1 shows a side view of the slider and the disk for this case. As can be seen from Fig. 1, the read/write element and the resistance heater are positioned at the trailing edge of the slider. Activating the resistance heater, the head disk clearance
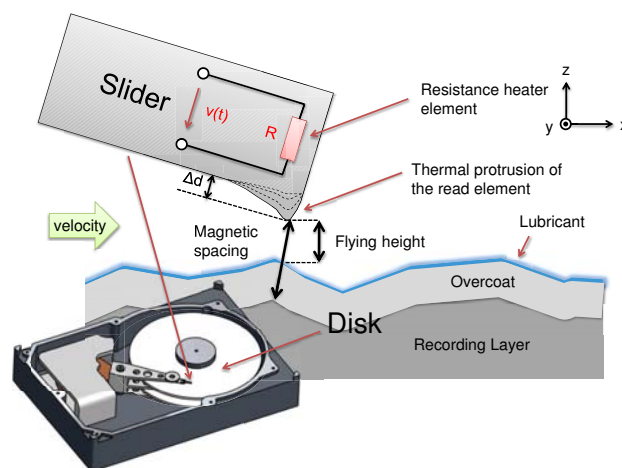

Fig. 1. Hard disk drive and side view of trailing edge of the slider with resistance heater element for thermal flying height control

can be reduced by Δd. Hence, the write current induced pole tip protrusion can be compensated by activating the resistance heater during reading. Secondly, tolerances during manufacturing of the head can be relaxed and flying height changes due to changes in environmental conditions during operation can be compensated. Thermal flying height control (TFC) is being applied in current disk
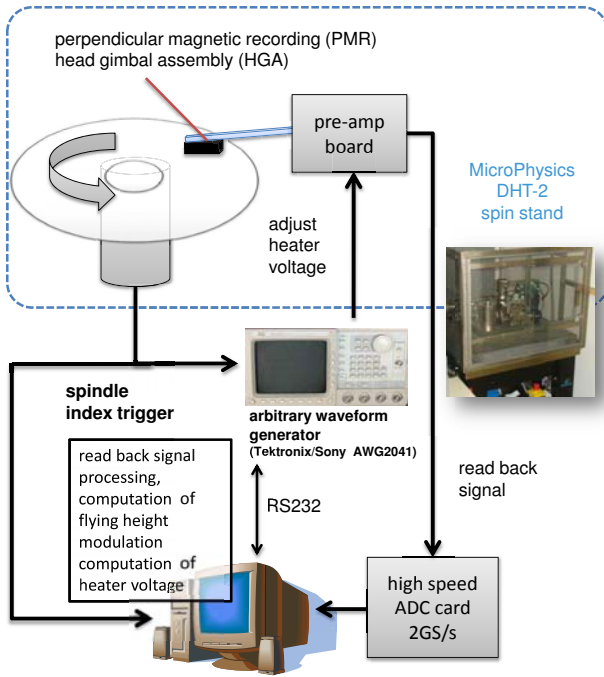
Fig. 2. Schematic of experimental spin stand set-up

drives in a "static sense", i.e., the power level applied to the heater is independent of the circumferential position of the slider over the disk. It is adjusted only depending on radial position, writing or reading operation and environmental conditions. However, the flying height varies in a repeatable manner (Xu et al. (2006)). Limited results are available on dynamically adjusting the TFC power to minimize flying height variations that occur along the circumference. One approach for dynamic TFC has been shown by Shiramatsu et al. (2008) where a feed forward methodology is used. An adaptive regulator scheme was proposed and simulated by Wu and Amara (2005) and experimental results using a piezo-electric actuator where recently given (Wu and Ben Amara (2010)). In the present paper, a different method of flying height control based on convex optimization will be proposed to solve the flying height variation minimization problem. We presented an initial approach to solving this problem at the APMRC 2010 in Singapore. Efficient solvers for those type of problems have been developed recently, which make real-time or nearly real-time applications feasible as shown by Mattingely and Boyd (2010). Hence, the optimal power profile to the heater element can be computed that minimizes repeatable circumferential variations of flying height.

2. EXPERIMENTAL SET-UP

Experimental data were obtained on a Disk-Head Tester (Microphysics spin stand model DHT-2) illustrated in the schematic in Fig. 2. The measurements were performed at a radius of 28 mm, a skew angle of 1.3 degrees and a rotational speed of 7200 rpm. The relative magnetic spacing (which is assumed to correspond to the relative flying height) is computed using the read back signal of the servo sectors on the disk and a modified Wallace spacing loss formula. Here, we consider A and B burst of a conventional amplitude based servo pattern and the
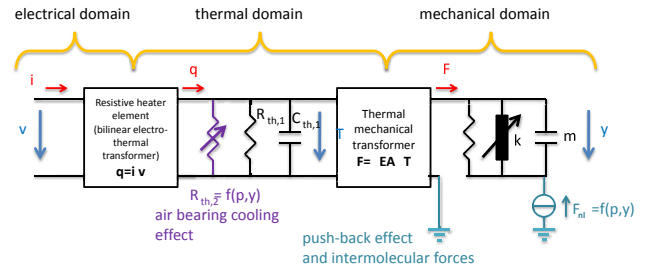

Fig. 3. Simplified network model of the resistance heater element including non-linear effects such as air-bearing cooling effect and push-back effect

flying height change Δz is computed as in Boettcher et al. (2011) by

$$\Delta z = \frac{\lambda_1}{16\pi} \left(\ln \left(\Phi_{A1} + \Phi_{B1} \right) - 3 \ln \left(\Phi_{A3} + \Phi_{B3} \right) \right) \quad (1)$$

where $\Phi_{A,Bi}$ is the amplitude of the ith harmonic of the A and B burst, respectively, and λ_1 is the wavelength of the first harmonic. A 16 T pattern consisting of 8 "up" followed by 8 "down" magnetized perpendicularly oriented bits was employed as the servo pattern at a write frequency of 900 MHz which yields the first harmonic frequency at 56.25 MHz. The read back signal in the servo sectors was sampled at 2 GHz and a total number of 128 servo sectors corresponds to a sampling frequency of the flying height modulation of 15.36 kHz. An arbitrary waveform generator was used to apply the power profile to the heater. The spindle index signal was used as a trigger.

3. DYNAMIC MODELING OF THE HEATER RESPONSE

3.1 Modeling based on physical principles

To model the flying height variation induced by the thermal actuator based on physical principles is complicated and contains several effects that have been reported in the literature; a short overview is given in the following. A simplified network approach is shown in Fig. 3. The system ranges over three physical domains, i.e., electrical, thermal and mechanical). The voltage applied to the heater yields a resistive heating (Joule heating) of the heater element and its surrounding materials. This causes a thermal expansion and deformation of the air bearing surface which positions the read/write element closer to the disk as indicated in Fig. 1. There are several effects that counteract the thermally induced flying height reduction:

(1) Electrical domain: The resistance of the heater element changes as the temperature increases which changes the Joule heating effect
(2) Thermal domain: It was found by Chen and Bogy (2010) that the main heat exchange between the head and the disk is through heat conduction. As the distance between the thermal protrusion and the disk is reduced, the conductive heat exchange between the head and disk is increased due to a local pressure increase and a decrease in the mean free path of the air in the gap between thermal protrusion and disk. This is known as the air bearing cooling effect (Juang and Bogy (2007))
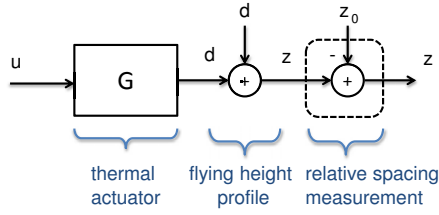
Fig. 4. Schematic of thermal actuator and flying height sensor

(3) Mechanical domain: A local increase in air bearing pressure causes the so-called push-back effect which is indicated in Fig.3 as a non-linear force acting on the output. Furthermore, in the close-contact regime, intermolecular and electrostatic forces will play a role as it has been shown by Gupta and Bogy (2005).

3.2 Data-based modeling approach

A data-based (black-box) modeling approach seems more feasible than a model derivation based on physical principles considering the presence of numerous parameter uncertainties. A schematic of the actuator and measurement system is shown in Fig. 4. Here, u represents the input power applied to the thermal actuator G. The flying height variation d is considered an unknown disturbance to be rejected by the thermal actuator. The absolute spacing z is not measurable in the experimental set-up described in section 2. Instead, the relative spacing to an initial unknown flying height z_0 is measured where

$$\Delta z = z - z_0 \qquad (2)$$

The contribution of the actuator to the flying height change can be estimated by performing two experiments with no (or only DC bias) input as a reference measurement and a second experiment using a persistently exciting input signal. A good choice is a step input signal. The step data can then be used to identify a discrete-time model of the actuator using the generalized realization algorithm (GRA) proposed by de Callafon et al. (2008). The GRA computes the state space matrices $\mathbf{A}$, $\mathbf{B}$ and $\mathbf{C}$ of a discrete-time model of the thermal actuator, illustrated in Fig. 4. The input/output relationship of the heater system shown in Fig. 4 can be written as

$$\mathbf{\Delta D} = \mathbf{HU} + \mathbf{E} \qquad (3)$$

where $\mathbf{\Delta D}$ is a Hankel matrix of the output signals, $\mathbf{U}$ is the input matrix and $\mathbf{H}$ is a Hankel matrix that contains the Markov parameters $g(k)$ defined by

$$g(k) = \begin{cases} \mathbf{D} & \text{for } k = 0 \\ \mathbf{CA^{k-1}B} & \text{for } k \geq 1 \end{cases} \qquad (4)$$

forming the matrix

$$\mathbf{H} = \mathbf{\Gamma\Omega} \qquad (5)$$

In (5), $\mathbf{\Gamma}$ and $\mathbf{\Omega}$ are the observability and controllability matrix, respectively, defined by

$$\mathbf{\Gamma} = \begin{bmatrix} \mathbf{C} \\ \mathbf{CA} \\ \vdots \\ \mathbf{CA^{k-1}} \end{bmatrix}, \qquad \mathbf{\Omega} = \begin{bmatrix} \mathbf{B} & \mathbf{AB} & \cdots & \mathbf{A^{k-1}B} \end{bmatrix} \qquad (6)$$

The matrix $\mathbf{E}$ contains the effect of past input signals multiplied by the Markov parameters of the system. For a step-function as an input, $\mathbf{E}$ is a row-wise listing of past output signals (de Callafon (2003)). A realization is performed based on the weighted Hankel matrix $\mathbf{R} = \mathbf{\Delta D} - \mathbf{E}$, allowing the use of step function input signals instead of impulse response measurements.

The measured step data are stored in a $N \times N$ Hankel Matrix

$$\mathbf{\Delta D} = \begin{bmatrix} \Delta d(1) & \Delta d(2) & \cdots & \Delta d(N) \\ \Delta d(2) & \Delta d(3) & \cdots & \Delta d(N+1) \\ \vdots & \vdots & \vdots & \vdots \\ \Delta d(N) & \Delta d(N+1) & \cdots & \Delta d(2N-1) \end{bmatrix} \qquad (7)$$

where N denotes the number of data points for each measurement. The vector Δd denotes the measured step response. The error matrix $\mathbf{E}$ is defined by

$$\mathbf{E} = \begin{bmatrix} \Delta d(0) & \cdots & \Delta d(0) \\ \vdots & \vdots & \vdots \\ \Delta d(N-1) & \cdots & \Delta d(N-1) \end{bmatrix} \qquad (8)$$

and the weighted Hankel matrix $\mathbf{R}$ is defined as

$$\mathbf{R} = \mathbf{\Delta D} - \mathbf{E} = \mathbf{HU} \qquad (9)$$

$\mathbf{R}$ has the same rank as $\mathbf{H}$. The matrix $\mathbf{R}$ is decomposed into a $N \times n$ matrix $\mathbf{R_1}$ and an $n \times N$ matrix $\mathbf{R_2}$, by using singular value decomposition. This decomposition enables choosing the rank n of the matrix, and, thus, the order of the estimated model. The singular value decomposition applied to $\mathbf{R}$ yields

$$\mathbf{R} = \mathbf{U\Sigma V^T} = \begin{bmatrix} U_\mathrm{n} & U_\mathrm{s} \end{bmatrix} \begin{bmatrix} \Sigma_\mathrm{n} & 0 \\ 0 & \Sigma_\mathrm{s} \end{bmatrix} \begin{bmatrix} V_\mathrm{n}^\mathrm{T} \\ V_\mathrm{s}^\mathrm{T} \end{bmatrix} \qquad (10)$$

In (10), $\mathbf{V}$ and $\mathbf{U}$ are unitary matrices, and Σ is a diagonal matrix that contains the singular values of the original matrix. The n largest singular values are stored in Σ_n while Σ_s contains the remaining smaller part. Using the singular value decomposition one can reduce $\mathbf{R}$ to a matrix with rank n:

$$\mathbf{R_n} = \mathbf{R_1 R_2} \qquad (11)$$

where $\mathbf{R_1}$ and $\mathbf{R_2}$ are defined by

$$\mathbf{R_1} = \mathbf{U_n \Sigma_n^{1/2}}, \quad \mathbf{R_2} = \mathbf{\Sigma_n^{1/2} V_n^T} \qquad (12)$$

With (6) we have $\mathbf{R_1} = \mathbf{\Gamma}$ and $\mathbf{R_2} = \mathbf{\Omega U}$ where $\mathbf{U}$ has full rank. The shifted version of $\mathbf{\Delta D}$ is denoted by $\mathbf{\bar{\Delta D}}$ and defined by

$$\mathbf{\bar{\Delta D}} = \begin{bmatrix} \Delta d(2) & \Delta d(3) & \cdots & \Delta d(N+1) \\ \Delta d(3) & \Delta d(4) & \cdots & \Delta d(N+2) \\ \vdots & \vdots & \vdots & \vdots \\ \Delta d(N+1) & \Delta d(N+2) & \cdots & \Delta d(2N) \end{bmatrix} \qquad (13)$$

and the corresponding shifted version of $\mathbf{R}$ can be described as

$$\mathbf{\bar{R}} = \mathbf{\bar{\Delta D}} - \mathbf{\bar{E}} \qquad (14)$$

From (4) and (6) it can be shown that the shifted version of $\mathbf{R}$ becomes

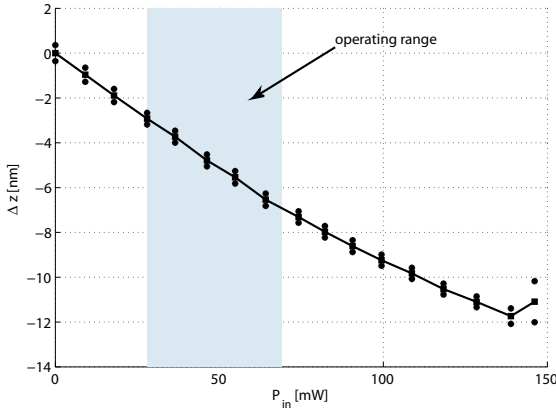$$\mathbf{\bar{R}} = \mathbf{\Gamma A \Omega U} = \mathbf{R_1 A R_2} \qquad (15)$$

Fig. 5. Touch down experiment showing the mean value of the flying height change over the circumference for the averaged (20 averages) flying height measurements

$\mathbf{R_1}$, $\mathbf{R_2}$ and $\bar{\mathbf{R}}$ are known. Hence, the state space matrix $\mathbf{A}$ can be estimated after computing the left and right inverse of (12):

$$\mathbf{R_1^*} = \mathbf{\Sigma}_n^{-1/2}\mathbf{U}_n^T, \ \mathbf{R_2^*} = \mathbf{V}_n\mathbf{\Sigma}_n^{-1/2} \quad (16)$$

The estimation for the state space matrix $\mathbf{A}$ yields

$$\mathbf{A} = \mathbf{R_1^*}\bar{\mathbf{R}}\mathbf{R_2^*} \quad (17)$$

From (6) it can be observed that the input matrix $\mathbf{B}$ can be described as the first column of $\mathbf{R_2}$ and that the first row of $\mathbf{R_1}$ forms the output matrix $\mathbf{C}$.

The feed-through term $\mathbf{D}$ contains only the first data point of the output signal after an input step, i.e., $\mathbf{D} = \Delta d(0)$. The D matrix could also be estimated by solving a least-square problem but in the present case it can also be set to zero as one sample time-delay can be assumed for the thermal actuator.

3.3 Modeling algorithm applied to experimental data

The described modeling procedure was applied to the heater element in the TFC slider. Voltage steps were applied to the heater element and the input power P was computed using $P = \frac{v^2}{R}$ assuming a fixed value for the heater resistance R. The step experiments were performed approximately 3 nm below the initial flying height after applying a bias voltage. Figure 5 shows a touchdown experiment considering the mean relative flying height over the circumference. It should be noted that the dynamic and static behavior of the thermal actuator is inherently non-linear and highly depends on the absolute spacing of the head over the disk as indicated in section 3.1. Therefore, we restrict ourselves to an operation range depicted in Fig. 5. Contact between the head and the disk is anticipated to occur between 11 and 12 nm below the initial flying height. Therefore, the minimum absolute flying height in the operating range is approximately 4 to 5 nm.

The results of the step experiments are shown in Fig. 6 where Fig. 6a) shows the reference input power and the step input power. The response can be seen in Fig. 6b). The squares represent the averaged values (20 averages)
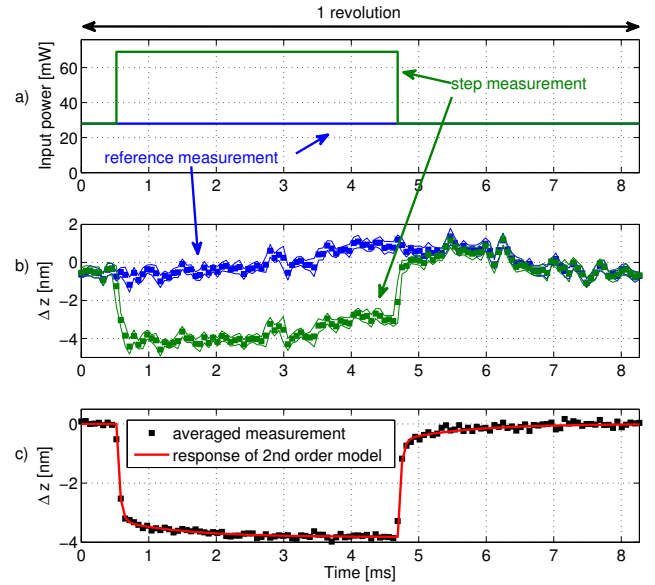

Fig. 6. Averaged spin stand measurement (20 averages): a) power input: reference, step. b) corresponding measured flying height variation (averaged values and standard derivation) c) identified 2nd order model and relative averaged spacing measurement
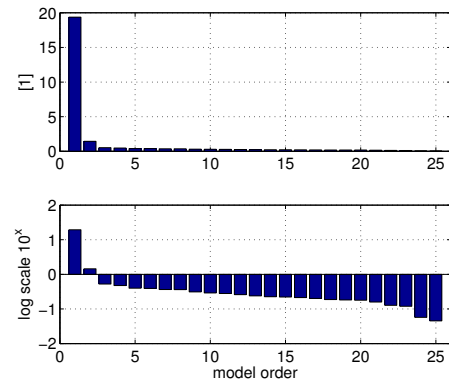

Fig. 7. Singular values of the weighted Hankel matrix

obtained at each of the 128 servo sectors and the lines represent the standard deviation. The response of the thermal actuator is the difference between both measurements in Fig. 6b) and is shown in Fig. 6c). It can be seen from Fig. 6c) that the actuator response consists of a fast and a slow mode.

A plot of the singular values of the weighted Hankel matrix $\mathbf{R}$ in (9) is shown in Fig. 7. Although the second singular value is much less significant than the first one, there is a considerable difference between the second and third singular value. Thus, this plot suggests the choice of a second order model. The model is given in discrete-time by

$$G(z) = \frac{-0.06161z + 0.05709}{z^2 - 1.172z + 0.2205} \quad (18)$$

For maximum read back performance, the operating range of the read/write element should be as close as possible to the disk. This introduces non-linear effects; which are beyond the scope of this paper. These effects will be of

interest for future work. Here, we restrict ourselves to show how repeatable flying height variations can be minimized for the operational range depicted in Fig. 5.

4. COMPUTING OPTIMAL POWER PROFILE

4.1 Development of the optimization algorithm

If the protrusion profile generated by the thermal actuator matches the inverse of the flying height modulation profile, a constant flying height is obtained. The computation of the power profile based on the inverse is not trivial as the inverse of the model is not necessarily stable and in addition non-causal. Furthermore, the fact that the control signals are limited could not be taken into account. Shiramatsu et al. (2008) limit the control signals through filtering, whereas in this paper, we explicitly compute control signals considering imposed amplitude bounds. The task is formulated as a convex optimization problem where the flying height modulation is minimized in a 2-norm sense. The direct computation of a feed forward profile makes the design of a feed forward filter redundant.

The second order model of the identified heater actuator is written in state space form as

$$x(k+1) = Ax(k) + Bu(k)$$
$$\Delta d(k) = Cx(k) \tag{19}$$

where A, B and C follow from the identification procedure described in section 3.

Following Goodwin et al. (2005), we can recursively rewrite the actuator output Δd as

$$\Delta d(0) = Cx(0)$$
$$\Delta d(1) = CAx(0) + CBu(0)$$
$$\Delta d(2) = CA^2x(0) + CABu(0) + CBu(1)$$
$$\vdots \tag{20}$$
$$\Delta d(N-1) = CA^{N-1}x(0) + \sum_{i=1}^{N-1} CA^{N-i}Bu(i-1)$$

or in matrix form

$$\mathbf{\Delta d} = \mathbf{\Psi u} \tag{21}$$

where

$$\mathbf{\Psi} = \begin{bmatrix} 0 & 0 & 0 \cdots & 0 \\ CB & 0 & 0 \cdots & 0 \\ CAB & CB & 0 \cdots & 0 \\ \vdots & \vdots & \vdots \ddots & \vdots \\ CA^{N-2}B & CA^{N-3}B & \cdots & 0 \\ CA^{N-1}B & CA^{N-2}B & \cdots & CB \end{bmatrix} \tag{22}$$

The initial value of the state $x(0)$ is set to zero. Based on this definition, the following optimization problem can be stated:

$$\min_{\mathbf{u}} \|\mathbf{\Psi u} + \mathbf{d} - \inf(\mathbf{d}) - \Delta z_0\|_2$$
$$\text{subject to} \quad \mathbf{u} \leq \mathbf{u_{max}} \tag{23}$$
$$\mathbf{u} \geq \mathbf{u_{min}}$$

The motivation to pose the optimization problem in (23) is as follows. A flying height lower than the infimum of
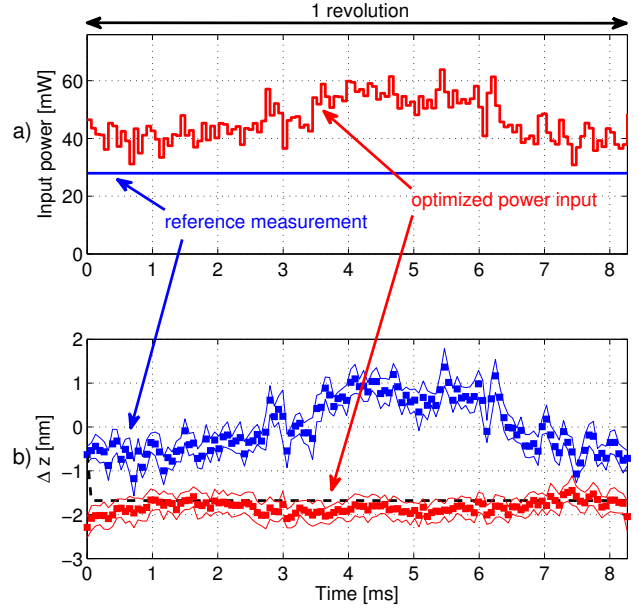

Fig. 8. Averaged spin stand measurement (20 averages): a) power input: reference signal, optimized signal. b) corresponding measured flying height variation (averaged values and standard derivation)

the flying height modulation d is desired as no negative power can be applied to the heater. An additional spacing parameter $\Delta z_0 > 0$ is defined to be able to lower the flying height. Linear constraints on the input power u are imposed through energy and design limitations on the thermal actuator reflected by $\mathbf{u_{max}}$ and $\mathbf{u_{min}}$. In a HDD drive application, Δz_0 could be increased until the minimum stable flying height is reached. Minimizing the Euclidean norm as in (23) is equivalent to minimizing the Euclidean norm squared (Boyd and Vandenberghe (2004)).

The problem can be reformulated as a quadratic programming problem or a semidefinite programming problem. For no or very loose constraints on the actuator signal, the problem can be reduced to a conventional least-squares estimation problem.

4.2 Optimization algorithm applied to experimental set-up

The model of the heater element that was estimated in section 3 and (23) were used to compute an optimized power input signal. The CVX software package developed by Grant and Boyd (2010) was used to solve the optimization problem. Δz_0 was chosen to be 0.5 nm as a bias voltage was already applied to the heater. This yields an approximate absolute flying height of $7 - 8$ nm. The measurements are shown in Fig. 8 The estimated flying height based on the optimization is indicated by the dashed line which is perfectly flat. The measured optimized flying height profile depicted in Fig. 2b) shows small variations. However, the variations are much smaller in amplitude than the initial reference profile also shown in this figure.

5. CONCLUSIONS

A discrete-time dynamic model of a thermal flying height actuator in a hard disk drive was identified using step

experiments and a generalized realization algorithm. It was found that the heater response can be modeled sufficiently well with a second order model that captures both a fast and slow time constant observed in the heater step response. It was shown how convex optimization techniques can be used to minimize circumferential flying height variations in a disk drive significantly based on the identified heater actuator model. Spin stand experiments showed that the flying height variation was reduced to about 1/3 in maximum-minimum value difference compared to the initial reference measurement where no power optimization was performed. Since the proposed method is a true feed forward technique it cannot be applied to compensating non-repeatable flying height variations. However, repeatable flying height variations can be compensated. The prediction is in good agreement with experimental results. Small variations can be explained with modeling errors. Furthermore, the flying height measurement used in this study had a sampling rate of 15.36 kHz and might therefore be potentially aliased. Higher sampling rates might yield even better results. The thermal actuator was found to be very fast and seems promising for flying height adjustment up to several kHz. The presented algorithms on heater dynamics modeling and input power optimization are not computational expensive and could be implemented in the firmware of the hard disk drive. This might enable an increase in durability and reliability of the drive while decreasing flying height and bit error rate. The identified linear model of the heater becomes invalid in the close-contact regime due to non-linearities. Future work should involve non-linear modeling approaches and adaptive feed forward approaches to minimize the flying height while maintaining a minimum in flying height variations.

ACKNOWLEDGEMENTS

REFERENCES

Boettcher, U., Lacey, C., Li, H., Amemiya, K., de Callafon, R., and Talke, F. (2011). Servo signal processing for flying height control in hard disk drives. *Microsystem Technologies, Special Issue, Proceedings of the ISPS.* doi:10.1007/s00542-010-1193-7.

Boyd, S. and Vandenberghe, L. (2004). *Convex Optimization.* Cambridge University Press, New York.

Chen, D. and Bogy, D. (2010). Simulation of static flying attitudes with different heat transfer models for a flying-height control slider with thermal protrusion. *Tribology Letters*, 40, 31–39. 10.1007/s11249-009-9551-2.

de Callafon, R.A., Moaveni, B., Conte, J.P., He, X., and Udd, E. (2008). General realization algorithm for modal identification of linear dynamic systems. *Journal of Engineering Mechanics*, 134(9), 712–722. doi: 10.1061/(ASCE)0733-9399(2008)134:9(712).

de Callafon, R. (2003). Estimating parameters in a lumped parameter system with first principle modeling and dynamic experiments. *Proceedings of 13th IFAC Symposium on System Identification,Rotterdam, the Netherlands*, 1613 – 1618.

Goodwin, G., Seron, M., and de Dona, J. (2005). *Constrained Control and Estimation: An Optimization Approach.* Springer Verlag, London.

Grant, M. and Boyd, S. (2010). CVX: Matlab software for disciplined convex programming, version 1.21. http://cvxr.com/cvx.

Gupta, V. and Bogy, D. (2005). Dynamics of sub-5-nm air-bearing sliders in the presence of electrostatic and intermolecular forces at the head-disk interface. *Magnetics, IEEE Transactions on*, 41(2), 610 – 615. doi: 10.1109/TMAG.2004.838062.

Harker, J.M., Brede, D.W., Pattison, R.E., Santana, G.R., and Taft, L.G. (1981). A quarter century of disk file innovation. *IBM Journal of Research and Development*, 25(5), 677 –690. doi:10.1147/rd.255.0677.

Hsia, Y.T. (2006). The ever shrinking hard disk drive and its components: What are the challenges? *Micro-NanoMechatronics and Human Science, 2006 International Symposium on*, 1 –2. doi: 10.1109/MHS.2006.320313.

Juang, J.Y. and Bogy, D.B. (2007). Air-bearing effects on actuated thermal pole-tip protrusion for hard disk drives. *Journal of Tribology*, 129(3), 570–578. doi: 10.1115/1.2736456.

Mächtle, P., Berger, R., Dietzel, A., Despont, M., Haberle, W., Stutz, R., Binnig, G., and Vettiger, P. (2001). Integrated microheaters for in-situ flying-height control of sliders used in hard-disk drives. *Micro Electro Mechanical Systems, 2001. MEMS 2001. The 14th IEEE International Conference on*, 196 –199. doi: 10.1109/MEMSYS.2001.906512.

Mattingely, J. and Boyd, S. (2010). Real-time convex optimization in signal processing. *Signal Processing Magazine, IEEE*, 27(3), 50 –61. doi: 10.1109/MSP.2010.936020.

Shiramatsu, T., Atsumi, T., Kurita, M., Shimizu, Y., and Tanaka, H. (2008). Dynamically controlled thermal flying-height control slider. *Magnetics, IEEE Transactions on*, 44(11), 3695 –3697. doi: 10.1109/TMAG.2008.2002626.

Tang, Y., Hong, S.Y., Kim, N.Y., and Che, X. (2007). Overview of fly height control applications in perpendicular magnetic recording. *Magnetics, IEEE Transactions on*, 43(2), 709 –714. doi:10.1109/TMAG.2006.888363.

Wu, Z. and Amara, F. (2005). Adaptive regulation of the flying height in hard disk drives. In *Control Applications, 2005. CCA 2005. Proceedings of 2005 IEEE Conference on*, 1146 –1151. doi:10.1109/CCA.2005.1507285.

Wu, Z. and Ben Amara, F. (2010). Adaptive regulation in switched bimodal systems: An experimental evaluation. *Control Systems Technology, IEEE Transactions on*, 18(4), 885 –895. doi:10.1109/TCST.2009.2030789.

Xu, J., Shimizu, Y., and Su, L. (2006). Drive level measurement of flying height modulation and control of slider disk contact. *Tribology Letters*, 24, 159–162. 10.1007/s11249-006-9153-1.

Yeack-Scranton, C., Khanna, V., Etzold, K., and Praino, A. (1990). An active slider for practical contact recording. *Magnetics, IEEE Transactions on*, 26(5), 2478 –2483. doi:10.1109/20.104770.